



**HAL**  
open science

## High resolution threshold photoelectron spectrum and autoionization processes of S<sub>2</sub> up to 15.0 eV

Helgi Rafn Hrodmarsson, Gustavo A Garcia, Laurent Nahon, Jean-Christophe Loison, Bérenger Gans

► **To cite this version:**

Helgi Rafn Hrodmarsson, Gustavo A Garcia, Laurent Nahon, Jean-Christophe Loison, Bérenger Gans. High resolution threshold photoelectron spectrum and autoionization processes of S<sub>2</sub> up to 15.0 eV. Journal of Molecular Spectroscopy, 2021, pp.111533. 10.1016/j.jms.2021.111533 . hal-03365531

**HAL Id: hal-03365531**

**<https://hal.science/hal-03365531>**

Submitted on 5 Oct 2021

**HAL** is a multi-disciplinary open access archive for the deposit and dissemination of scientific research documents, whether they are published or not. The documents may come from teaching and research institutions in France or abroad, or from public or private research centers.

L'archive ouverte pluridisciplinaire **HAL**, est destinée au dépôt et à la diffusion de documents scientifiques de niveau recherche, publiés ou non, émanant des établissements d'enseignement et de recherche français ou étrangers, des laboratoires publics ou privés.

# High resolution threshold photoelectron spectrum and autoionization processes of S<sub>2</sub> up to 15.0 eV

Helgi Rafn Hrodmarsson<sup>1,2\*</sup>, Gustavo A. Garcia<sup>1</sup>, Laurent Nahon<sup>1</sup>, Jean-Christophe Loison<sup>3</sup>,  
Bérenger Gans<sup>4</sup>

<sup>1</sup> *Synchrotron SOLEIL, L'Orme des Merisiers, St Aubin, BP 48, Gif sur Yvette, France*

<sup>2</sup> *Current address: Laboratory for Astrophysics, Leiden Observatory, Leiden University, PO  
Box 9513, NL-2300 RA Leiden, The Netherlands*

<sup>3</sup> *ISM, Université Bordeaux 1, CNRS, 351 cours de la Libération, 33405 Talence Cedex,  
France*

<sup>4</sup> *Institut des Sciences Moléculaires d'Orsay, CNRS, Université Paris-Saclay, 91405 Orsay,  
France*

Total number of pages in manuscript: 22

Tables: 4

Figures: 6

\*Correspondence should be addressed to:

Helgi Rafn Hrodmarsson

Permanent address:

Niels Bohrweg 2, 2333CA, Leiden. The Netherlands.

Laboratory for Astrophysics, Leiden Observatory, Leiden University, PO Box 9513, NL-2300  
RA.

E-mail: hr.hrodmarsson@gmail.com

## Abstract

VUV photoionization dynamics of the S<sub>2</sub> molecule were re-investigated from threshold up to 15.0 eV, using synchrotron radiation coupled with double imaging photoelectron/photoion coincidence featuring high resolution capabilities. We measured the first threshold photoelectron spectrum of S<sub>2</sub> achieving higher resolution than previous literature to derive accurate spectroscopic constants for a few electronic states of the cation including the X<sup>2</sup>Π<sub>Ω<sub>g</sub> ground state and the a<sup>4</sup>Π<sub>u</sub>, b<sup>4</sup>Σ<sub>g</sub><sup>-</sup>, and B<sup>2</sup>Σ<sub>g</sub><sup>-</sup> states. We also recorded the total ion yield for S<sub>2</sub> up to a photon energy of 15.0 eV which, combined with the threshold photoelectron spectrum, led to the assignment of various autoionizing Rydberg series.</sub>

## INTRODUCTION

Sulfur and its chemistry are not only an integral component of biochemical processes [1] but are omnipresent in the interstellar medium as well [2]. Neutral S<sub>2</sub> has been found in cometary comae [3,4], on Jupiter near the G impact site after the collision of Shoemaker-Levy 9 [5], in volcanic plumes on Io [6,7], and has been invoked as a contributor to stratospheric heating of hot Jupiters [8]. However, somewhat intriguingly, in primitive molecular clouds and star-forming regions, sulfur is increasingly depleted [9,10]. An abundance of sulfur-bearing molecules has been detected recently in the interstellar medium [11–15], but all-together it does not sufficiently account for the apparently missing sulfur. A theory gaining traction presumes that sulfur collects on interstellar dust grains where it is processed by UV and X-rays to form universal sulfur sinks such as S<sub>8</sub> [16]. In this context it is important to revisit the photoionization of the sulfur dimer, S<sub>2</sub>, as it is a potentially important reactive intermediate in interstellar regions whose chemistry is driven by UV and X-ray radiation.

Since the recording of the first photoelectron spectra of the S<sub>2</sub> diradical [17,18], the spectroscopy of the S<sub>2</sub><sup>+</sup> cation has been explored by means of flowing afterglow [19–21], electron impact ionization [22], optical spectroscopy [23], photoluminescence in Ne matrices [24], and absorption spectroscopy of sulfur-doped silica glass [25]. The photoionization efficiency (PIE) curve of S<sub>2</sub> was measured up to 20.7 eV by Liao and Ng [26] and theoretical efforts pertaining to the ground state and excited states of the S<sub>2</sub><sup>+</sup> radical have been recently summarized [27]. Experimental efforts to study breakdown products from the interaction of disulfide bridge-containing molecules with high energy photons found that S<sub>2</sub><sup>+</sup> was persistently formed at energies in the low-keV regime, attesting its chemical stability [28].

The work of Rosinger *et al.* [22], revealed several features in the recorded ionization efficiency curves which were attributed to autoionization processes, and Liao and Ng [26] further inspected these autoionizing features which had clearly visible bands in the PIE curve

35 of S<sub>2</sub>. While they noted that it was likely that these vibrational bands could be grouped into  
36 more than one vibrational progression, only a handful were assigned.

37 By using the double-imaging photoelectron/photoion coincidence (i<sup>2</sup>PEPICO)  
38 technique [29] coupled with synchrotron radiation we present the threshold photoelectron  
39 spectra (TPES) and total ion yield (TIY) from threshold up to 15.0 eV. The TIY allows us to  
40 assign features corresponding to autoionization of neutral Rydberg states converging to  
41 different vibronic states of S<sub>2</sub><sup>+</sup>, which are in turn assigned using the TPES. We also present a  
42 two-dimensional kinetic energy vs photon energy matrix of the cation signal which further  
43 evidences these ionization dynamics.

44

## 45 **METHODOLOGIES**

46 Experiments were performed on the DESIRS VUV undulator beamline [30] located at the third  
47 generation French national synchrotron facility SOLEIL. The experimental apparatus that was  
48 used is the permanent molecular beam end-station SAPHIRS [31] which is equipped with the  
49 i<sup>2</sup>PEPICO spectrometer DELICIOUS3 [32]. Ions and electrons were detected in coincidence  
50 with an imaging Wiley-McLaren time-of-flight analyzer and a velocity map imaging (VMI)  
51 setup, respectively. The DESIRS beamline monochromator was set to deliver a photon energy  
52 resolution of 3 meV at 8 eV and a gas filter [33] upstream was filled with either krypton or  
53 argon depending on the energy range, to filter out higher harmonics of the beamline undulator,  
54 OPHELIE2 [34].

55 S<sub>2</sub> was produced by recombination of S atoms which were formed by double H-  
56 abstraction from H<sub>2</sub>S in a flow-tube placed inside the SAPHIRS chamber [35]. The S<sub>2</sub> diradicals  
57 were produced as secondary products of a process initially set up to produce SH radicals. All  
58 the experimental parameters pertaining to this experiment have been described in detail  
59 previously [36].

60 Three energy scans were performed; one from threshold up to 12.0 eV and two scans  
61 from 11.9 eV to 15.0 eV, one in which the particle acceleration was achieved with a DC electric  
62 field of 53 V·cm<sup>-1</sup> and one where it was increased to 177 V·cm<sup>-1</sup> to collect all coincident events  
63 related to S<sub>2</sub><sup>+</sup> ions up to 15 eV. Autoionizing resonances corresponding to transitions in neutral  
64 atomic sulfur were used for absolute photon energy calibration. This does not account for the  
65 Stark shift in the recorded TPES which is induced by the applied DC electric field to achieve  
66 particle acceleration. The Stark shift can be quantified by calculating  $6\sqrt{F}$  (in cm<sup>-1</sup> with  $F$   
67 denoting the electric field in V·cm<sup>-1</sup>) [29] which gives a shift of 5.4 meV in the case of the 53

68 V·cm<sup>-1</sup> scans that were used to record the TPES. All the ionization thresholds given in this  
 69 paper have been corrected by this field-induced shift.

70 At each photon energy of the scans, the recorded images were inverted [37] so the  
 71 electron signal detected in coincidence with <sup>32</sup>S<sub>2</sub> can be obtained as a function of electron kinetic  
 72 energy and photon energy in a two-dimensional matrix representation (see below). Therein,  
 73 diagonal signals correspond to direct ionizations into a cationic state where the kinetic energy  
 74 of the produced photoelectrons increases linearly with excess energy. Vertical lines, however,  
 75 evidence excitations to Rydberg states that are resonant with the photon energy, which  
 76 autoionize according to the different couplings to the cation states.

77 The threshold photoelectron spectrum (TPES) is obtained by integrating the intensities  
 78 along the diagonal lines (constant ionic states) up to a relatively small value of kinetic  
 79 energy [38]. For this experiment, the best signal to background ratio was found for an electron  
 80 kinetic energy cut-off (Ele KE<sub>max</sub>) value of 5 meV.

81 Mass signals corresponding to  $m/z = 65$  (<sup>33</sup>S<sup>32</sup>S) and  $m/z = 66$  (<sup>34</sup>S<sup>32</sup>S, the <sup>33</sup>S<sub>2</sub>  
 82 contribution is negligible) were clearly visible [36] and the TPES from these mass channels are  
 83 analyzed for the X<sup>2</sup>Π<sub>Ω,g</sub> ground state. As for the excited ionic states, the observed peak  
 84 positions in the recorded TPES are indistinguishable in all mass channels which forbids any  
 85 differentiation in the analysis of the ionic states of <sup>33</sup>S<sup>32</sup>S and <sup>34</sup>S<sup>32</sup>S, and in <sup>32</sup>S<sub>2</sub>. Furthermore,  
 86 as the <sup>33</sup>S<sup>32</sup>S and <sup>34</sup>S<sup>32</sup>S signals were significantly weaker than that of the  $m/z = 64$  channel,  
 87 their TPES were created with larger Ele KE<sub>max</sub> values, namely 10 meV which also results in  
 88 larger errors of their spectroscopic parameters as will be discussed in section 3.2.

89

## 90 RESULTS AND DISCUSSION

### 91 3.1 Valence Electron Configurations of S<sub>2</sub> and S<sub>2</sub><sup>+</sup>

92 Photoionization of homonuclear chalcogens (O<sub>2</sub>, S<sub>2</sub>, etc.) gives rise to multiplex photodynamics  
 93 which can be attributed to the nature of being open shell triplet molecular systems. Here we  
 94 present the electron configurations of the neutral and ionized S<sub>2</sub> to assist the reader through the  
 95 assignments of the total ion yield curve (section 3.2) and the TPES (section 3.3).

96 The electron configuration of neutral S<sub>2</sub> in the ground state (X<sup>3</sup>Σ<sub>g</sub><sup>-</sup>) is the following:

$$97 \quad [S_2]: (\sigma_{3s})^2(\sigma_{3s}^*)^2(\sigma_{3p})^2(\pi_{3p})^4(\pi_{3p}^*)^2$$

98 and for the ground state (X<sup>2</sup>Π<sub>Ω,g</sub>) of the S<sub>2</sub><sup>+</sup> cation, the electron configuration is obtained by  
 99 removing an electron from the π<sub>3p</sub><sup>\*</sup> orbital:

$$100 \quad [S_2^+]: (\sigma_{3s})^2(\sigma_{3s}^*)^2(\sigma_{3p})^2(\pi_{3p})^4(\pi_{3p}^*)$$

101 The first two excited states of the  $S_2^+$  cation, namely  $a^4\Pi_u$  and  $A^2\Pi_u$ , are obtained by removing  
 102 an electron from the  $\pi_{3p}$  orbital, spin down and spin up, respectively. As seen in Table 1, four  
 103 different Rydberg series converging to each of the  $a^4\Pi_u$  and  $A^2\Pi_u$  states are obtained by  
 104 promoting an electron from a p orbital, to either s ( $\sigma_g$ ) or d ( $\sigma_g, \pi_g, \delta_g$ ) Rydberg orbitals.

105 We note that the approximate quantum defects in the Rydberg series of free atomic  
 106 sulfur are  $\delta = 2.0$  for  $ns$ , 1.6 for  $np$ , and 0.3 for  $nd$  orbitals [40] so that it is not unreasonable to  
 107 expect similar trends for  $S_2$  as has been done previously [26].

108

109 **Table 1.** Summary of the valence electron configurations of the cationic states of  $S_2^+$  and the  
 110 Rydberg states of the neutral  $S_2$  that converge to them.

$S_2^+$	$S_2$
Ground state – $X^2\Pi_{\Omega_g}(\Omega = 1/2, 3/2)$ : $(\sigma_{3s})^2(\sigma_{3s}^*)^2(\sigma_{3p})^2(\pi_{3p})^4(\pi_{3p}^*)^2$	Ground state – $X^3\Sigma_g^-$ : $(\sigma_{3s})^2(\sigma_{3s}^*)^2(\sigma_{3p})^2(\pi_{3p})^4(\pi_{3p}^*)^2$
$a^4\Pi_u$ state: $(\sigma_{3s})^2(\sigma_{3s}^*)^2(\sigma_{3p})^2(\pi_{3p})^3(\pi_{3p}^*)^2$	$(\sigma_{3s})^2(\sigma_{3s}^*)^2(\sigma_{3p})^2(\pi_{3p})^3(\pi_{3p}^*)^2ns\sigma_g$ $(\sigma_{3s})^2(\sigma_{3s}^*)^2(\sigma_{3p})^2(\pi_{3p})^3(\pi_{3p}^*)^2nd\sigma_g$ $(\sigma_{3s})^2(\sigma_{3s}^*)^2(\sigma_{3p})^2(\pi_{3p})^3(\pi_{3p}^*)^2nd\delta_g$ $(\sigma_{3s})^2(\sigma_{3s}^*)^2(\sigma_{3p})^2(\pi_{3p})^3(\pi_{3p}^*)^2nd\pi_g$
$A^2\Pi_u$ state: $(\sigma_{3s})^2(\sigma_{3s}^*)^2(\sigma_{3p})^2(\pi_{3p})^3(\pi_{3p}^*)^2$	$(\sigma_{3s})^2(\sigma_{3s}^*)^2(\sigma_{3p})^2(\pi_{3p})^3(\pi_{3p}^*)^2ns\sigma_g$ $(\sigma_{3s})^2(\sigma_{3s}^*)^2(\sigma_{3p})^2(\pi_{3p})^3(\pi_{3p}^*)^2nd\sigma_g$ $(\sigma_{3s})^2(\sigma_{3s}^*)^2(\sigma_{3p})^2(\pi_{3p})^3(\pi_{3p}^*)^2nd\delta_g$ $(\sigma_{3s})^2(\sigma_{3s}^*)^2(\sigma_{3p})^2(\pi_{3p})^3(\pi_{3p}^*)^2nd\pi_g$
$b^4\Sigma_g^-$ state: $(\sigma_{3s})^2(\sigma_{3s}^*)^2(\sigma_{3p})(\pi_{3p})^4(\pi_{3p}^*)^2$	$(\sigma_{3s})^2(\sigma_{3s}^*)^2(\sigma_{3p})(\pi_{3p})^4(\pi_{3p}^*)^2np\sigma_u$ $(\sigma_{3s})^2(\sigma_{3s}^*)^2(\sigma_{3p})(\pi_{3p})^4(\pi_{3p}^*)^2np\pi_u$
$B^2\Sigma_g^-$ state: $(\sigma_{3s})^2(\sigma_{3s}^*)^2(\sigma_{3p})(\pi_{3p})^4(\pi_{3p}^*)^2$	$(\sigma_{3s})^2(\sigma_{3s}^*)^2(\sigma_{3p})(\pi_{3p})^4(\pi_{3p}^*)^2np\sigma_u$ $(\sigma_{3s})^2(\sigma_{3s}^*)^2(\sigma_{3p})(\pi_{3p})^4(\pi_{3p}^*)^2np\pi_u$

111

112 The next two excited states of  $S_2^+$  are  $b^4\Sigma_g^-$  and  $B^2\Sigma_g^-$ . Their electron configurations  
 113 result from removing an electron from the  $\sigma_{3p}$  orbital, spin down and spin up respectively,  
 114 meaning that the Rydberg states converging to the b/B states require promoting an electron from

115 a  $\sigma$  binding p orbital and thus, the Rydberg states converging to the  $b^4\Sigma_g^-$  &  $B^2\Sigma_g^-$  states can  
116 have two possible electron configurations (Table 1).

117 Apart from the cationic states presented in Table 1, there are several other states that  
118 have been predicted by Yu *et al.* [27], namely,  $1^6\Sigma_u^+$ ,  $1^4\Sigma_g^+$ ,  $1^2\Sigma_u^+$ ,  $1^4\Pi_g$ ,  $1^2\Sigma_g^+$ ,  $1^4\Delta_g$ ,  $1^6\Pi_g$ ,  
119  $1^6\Sigma_g^+$ ,  $1^4\Sigma_u^+$ ,  $1^4\Delta_u$ ,  $2^4\Pi_u$ ,  $1^4\Sigma_u^-$ , and  $2^4\Pi_g$ . The spectroscopic parameters of these states were  
120 calculated with onsets ranging from  $31854\text{ cm}^{-1}$  (3.9 eV) to  $50531\text{ cm}^{-1}$  (6.3 eV) above the  
121  $X^2\Pi_{\Omega, g}$  ground state, *i.e.*, above the  $B^2\Sigma_g^-$  state.

122

### 123 3.2 Total Ion Yield

124 The 2D matrices displaying the mass-filtered electron-ion coincidence signals pertaining to  $m/z$   
125 = 64 are presented in Figure 1. In the first scan from 9.2 – 12.0 eV, the  $X^2\Pi_{\Omega, g}$  is the ground  
126 state and the first excited state,  $a^4\Pi_u$ , is seen with an onset of 11.58 eV. The second scan which  
127 covers 11.9 – 15.0 eV, unravels three additional excited states, namely  $A^2\Pi_u$ ,  $b^4\Sigma_g^-$ , and  $B^2\Sigma_g^-$ .

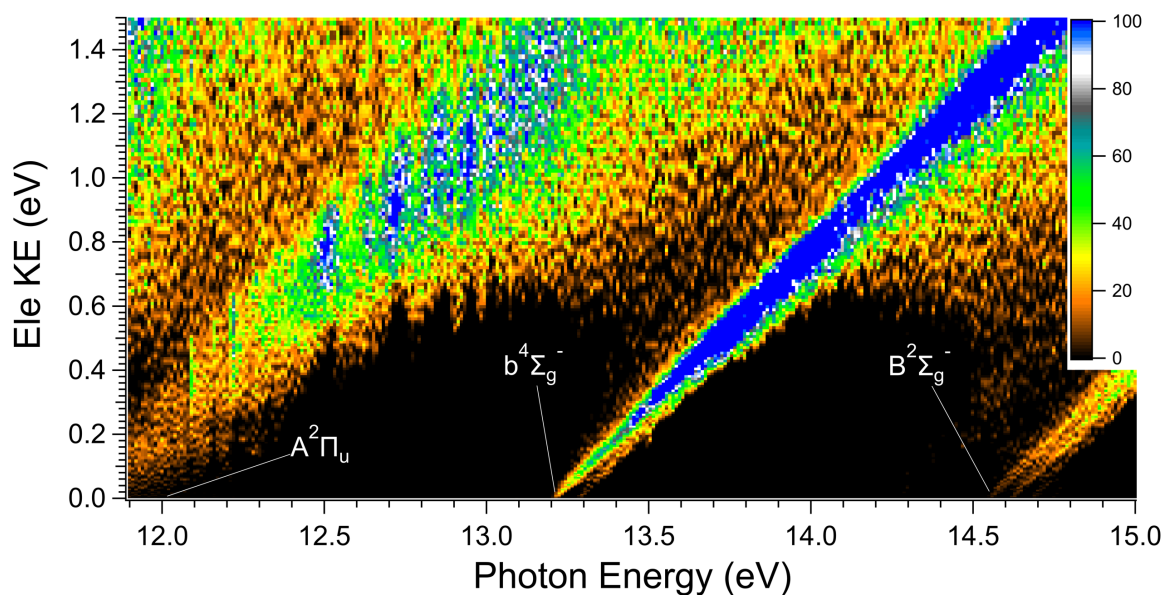
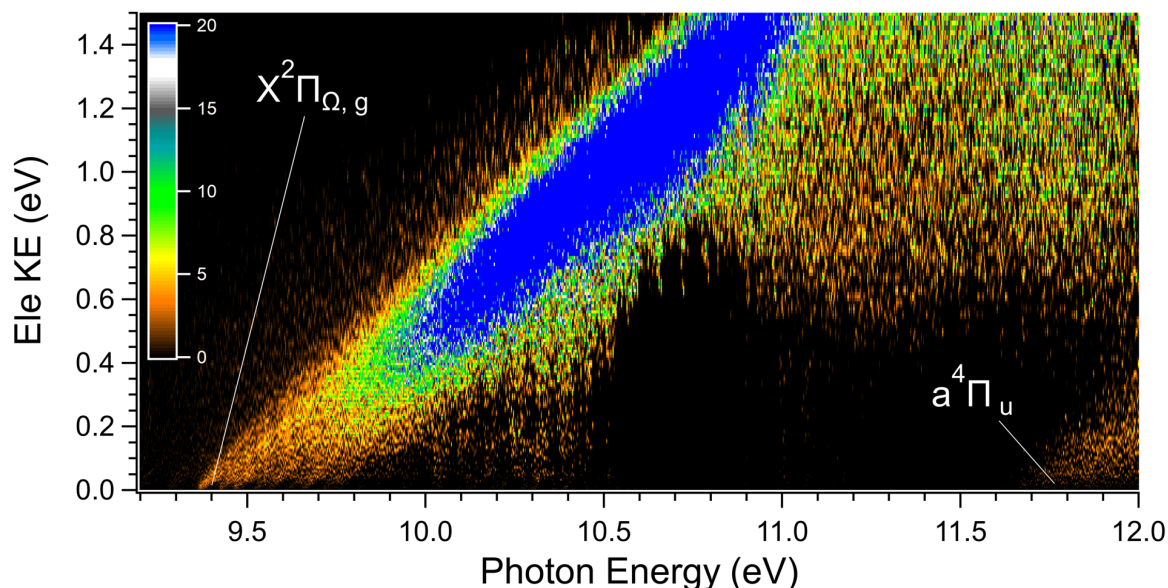
128 The 2D matrix in the upper panel of Figure 1 exhibits clear signs of autoionizing  
129 resonances that contribute to the ionization signals pertaining to the parent. These appear as  
130 vertical lines in the 2D matrix whereas direct ionization is observed as diagonal lines. Between  
131 10.0 and 10.5 eV, vertical lines are apparent in the 2D matrix. Above 10.5 eV, these signals  
132 seem to partly continue as tendrils dangling down from the direct ionization signal, whose shape  
133 resembles that of a diagonal cloud. Around 11.0 eV, the vertical lines become apparent again,  
134 albeit very weakly.

135 The sum of all of the ionic signals as a function of the photon energy in Figure 1 gives  
136 the total ion yield. The first attempt at assigning the autoionizing features in the rich total ion  
137 yield of  $S_2$  was made by Liao & Ng [26]. They assigned two Rydberg series converging to the  
138  $b^4\Sigma_g^-$  state with average quantum defects of 1.64 and 2.13 which would correspond to the  $[b^4\Sigma_g^-$   
139  $]np\pi_u$  and  $[b^4\Sigma_g^-]np\sigma_u$  Rydberg series, respectively, as outlined in section 3.1. They observed a  
140 plethora of other spectral structures but ultimately, their resolution forbade further assignments  
141 despite identifying structures relevant to Rydberg series converging to the ionic states of  $S_2^+$ .

142 Here, the recorded TPES (see section 3.3) can be used to guide the assignments and  
143 identify vibrational features in autoionizing Rydberg series converging to the corresponding  
144 ionic states.

145 Our total ion yield curve along with all of the relevant assignments is shown in Figure  
146 2 and Table 2 presents the assignments of the onsets of the Rydberg series detailed in Figure 2  
147 along with the calculated quantum defects which are representative of the Rydberg assignments.

148 Assignments labeled with an asterisk in Table 2 (\*) denote blended lines whose energy is best  
 149 estimated from the calculated quantum defect. The most notable is that of the  $[A^2\Pi_u]n s\sigma_g$   
 150 Rydberg series whose  $n = 5 - 8$  components are all blended with other series and hence their  
 151 assignment should be regarded as tentative despite the quantum defects being comparable.  
 152

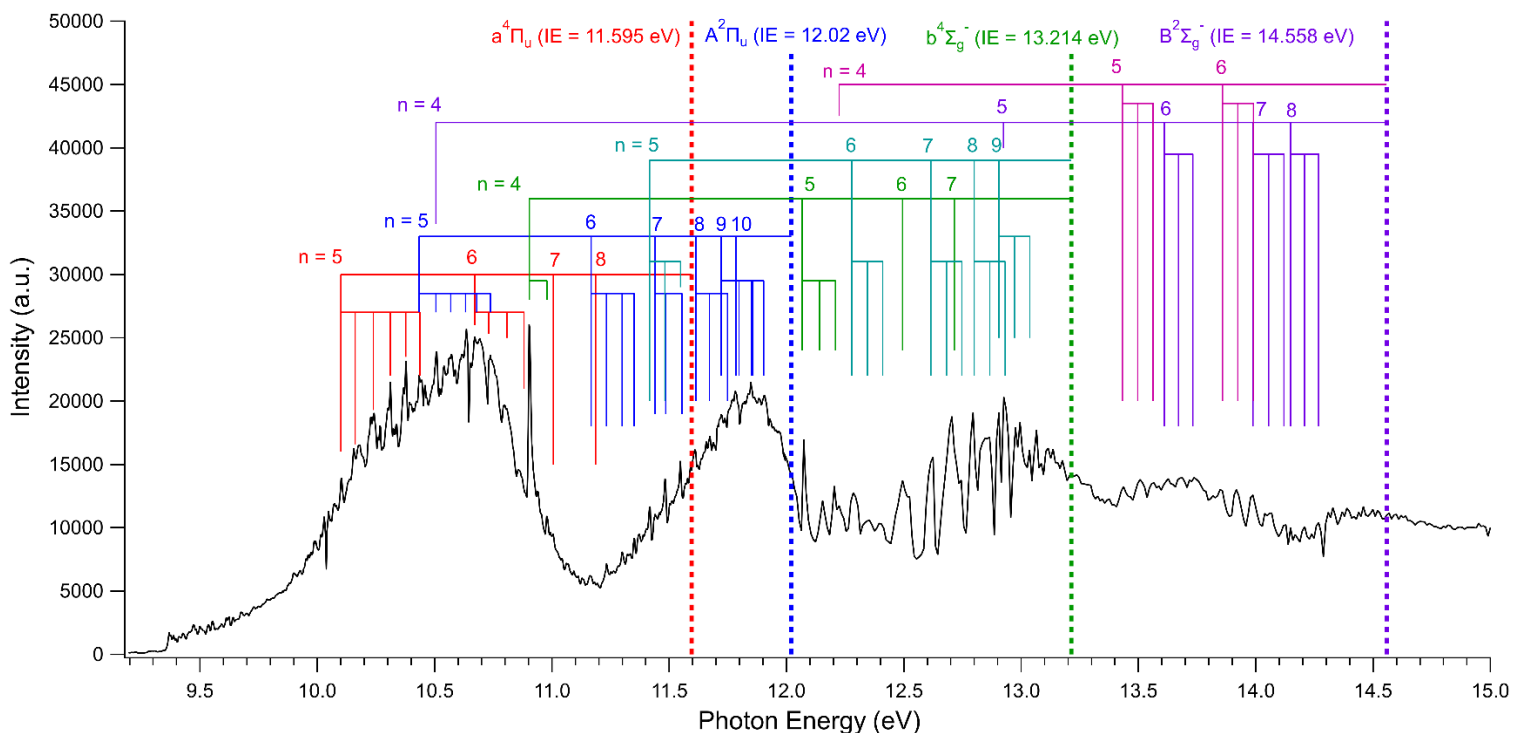


155 **Figure 1.** 2D matrices presenting the relative number of counts of electron-ion coincidences as  
 156 a function of electron kinetic energy ( $y$ -axis) and the photon energy ( $x$ -axis). The upper panel  
 157 presents the scan from 9.3 to 12.0 eV. The lower panel presents the scan from 11.9 to 15.0 eV.  
 158 The adiabatic ionization energies for the first five ionic states are presented and discussed in  
 159 section 3.3.

160



161 Sharp dips in the TIY are observed at 10.03 and 10.64 eV which correspond to krypton  
 162 absorption lines ( $4p^5 4s(3/2)_1^\circ \leftarrow 4p^6, ^1S_0$  and  $4p^5 4s'(1/2)_1^\circ \leftarrow 4p^6 ^1S_0$  series, respectively [41]).  
 163 For the scan up to 12 eV, krypton was used in the gas filter that was used to filter out higher  
 164 harmonics coming from the undulator. Argon was used in the gas filter for the second scan up  
 165 to 15 eV which is evidenced by several argon absorption lines, perhaps the most obvious one at  
 166 14.30 eV ( $3p^1 3d'(3/2)_1^\circ \leftarrow 3p^6 ^1S_0$  [42]).  
 167



169 **Figure 2.** Total ion yield curve in the photon energy range from 9.2 eV up to 15.0 eV. Different  
 170 Rydberg series (see Table 1) converging to ionic states are color-coded. The Rydberg series  
 171 converging to the  $a^4\Pi_u$  state is presented in red, the  $A^2\Pi_u$  state is presented in blue, the two  
 172 Rydberg series converging to the  $b^4\Sigma_g^-$  state are in green and teal, and the two Rydberg series  
 173 converging to the  $B^2\Sigma_g^-$  state are presented in purple and violet. In most cases we identify more  
 174 than one vibrational component in the assigned Rydberg series whose vibrational spacing are  
 175 of the same order as the ionic states assigned in the TPES (see section 3.3).  
 176

177 The assignments made by Liao & Ng to the two Rydberg series converging to the  $b^4\Sigma^-$   
 178 state principally occurred in the spectral region above 12.0 eV. Our assignment completely  
 179 reevaluates their assignment for two notable reasons. Firstly, the enhanced resolution allows us  
 180 to observe more structures in the TIY. Secondly, the recorded TPES allows us to more  
 181 accurately determine the appearance energies of the ionic states than in the PES study of  $S_2$  by

182 Dyke *et al.* [17] (section 3.3). This greatly influences the calculation of the quantum defects  
 183 which we used to guide our assignment to best fit with the recorded TIY.

184  
 185 **Table 2** Rydberg series of S<sub>2</sub> observed in the region 9.2 – 15.0 eV. Blended lines or tentative  
 186 assignments are denoted with an asterisk. We estimate that the uncertainty of other lines is equal  
 187 or better than 10 meV. Due to the broadened nature of the autoionizing lines, greater accuracy  
 188 cannot be expected in this case. Below each Rydberg series we present the corresponding  
 189 average quantum defect.

Energy		Principal quantum number	Experimentally-determined Quantum defect	Assignment
eV	cm <sup>-1</sup>	<i>n</i>	$\delta$	
10.096	81431	5	1.99	[a <sup>4</sup> Π <sub>u</sub> ]5sσ <sub>g</sub>
10.666	86028	6	2.17	[a <sup>4</sup> Π <sub>u</sub> ]6sσ <sub>g</sub>
11.00*	88730	7	2.21	[a <sup>4</sup> Π <sub>u</sub> ]7sσ <sub>g</sub>
11.18*	90182	8	2.27	[a <sup>4</sup> Π <sub>u</sub> ]8sσ <sub>g</sub>
Average $\delta = 2.16 \pm 0.12$				
10.43*	84116	5	2.08	[A <sup>2</sup> Π <sub>u</sub> ]5sσ <sub>g</sub>
11.16*	90028	6	2.02	[A <sup>2</sup> Π <sub>u</sub> ]6sσ <sub>g</sub>
11.48*	92569	7	1.99	[A <sup>2</sup> Π <sub>u</sub> ]7sσ <sub>g</sub>
11.64*	93900	8	2.00	[A <sup>2</sup> Π <sub>u</sub> ]8sσ <sub>g</sub>
11.741	94698	9	2.02	[A <sup>2</sup> Π <sub>u</sub> ]9sσ <sub>g</sub>
11.806	95222	10	2.02	[A <sup>2</sup> Π <sub>u</sub> ]10sσ <sub>g</sub>
Average $\delta = 2.02 \pm 0.03$				
10.898	87899	4	1.58	[b <sup>4</sup> Σ <sub>g</sub> <sup>-</sup> ]4pπ <sub>u</sub>
12.062	97287	5	1.56	[b <sup>4</sup> Σ <sub>g</sub> <sup>-</sup> ]5pπ <sub>u</sub>
12.500	100819	6	1.63	[b <sup>4</sup> Σ <sub>g</sub> <sup>-</sup> ]6pπ <sub>u</sub>
12.74*	102755	7	1.64	[b <sup>4</sup> Σ <sub>g</sub> <sup>-</sup> ]7pπ <sub>u</sub>
Average $\delta = 1.60 \pm 0.04$				
11.411	92037	5	2.25	[b <sup>4</sup> Σ <sub>g</sub> <sup>-</sup> ]4pσ <sub>u</sub>
12.273	98988	6	2.20	[b <sup>4</sup> Σ <sub>g</sub> <sup>-</sup> ]5pσ <sub>u</sub>

12.610	101707	7	2.25	$[b^4\Sigma_g^-]6p\sigma_u$
12.800	103239	8	2.27	$[b^4\Sigma_g^-]7p\sigma_u$
12.921	104215	9	2.19	$[b^4\Sigma_g^-]8p\sigma_u$
Average $\delta = 2.23 \pm 0.04$				
10.50*	84697	4	2.17	$[B^2\Sigma_g^-]4p\sigma_u$
12.90*	104046	5	2.14	$[B^2\Sigma_g^-]5p\sigma_u$
13.606	109740	6	2.22	$[B^2\Sigma_g^-]6p\sigma_u$
13.983	112780	7	2.14	$[B^2\Sigma_g^-]7p\sigma_u$
14.143	114071	8	2.27	$[B^2\Sigma_g^-]8p\sigma_u$
Average $\delta = 2.19 \pm 0.06$				
12.224*	98594	4	1.59	$[B^2\Sigma_g^-]4p\pi_u$
13.431	108329	5	1.53	$[B^2\Sigma_g^-]5p\pi_u$
13.858	111773	6	1.59	$[B^2\Sigma_g^-]6p\pi_u$
Average $\delta = 1.58 \pm 0.04$				

190

191            Though densely populated, we identify a number of Rydberg states in the spectral region  
192 between 10 and 11 eV. First of which is the vibrational progression of the  $[a^4\Pi_u]5s\sigma_g$  and  
193  $[a^4\Pi_u]6s\sigma_g$  states which have a very similar structure and vibrational profile as that of the  $a^4\Pi_u$   
194 state. Higher components of the  $[a^4\Pi_u]ns\sigma_g$  states can be identified but they are significantly  
195 weaker.

196            The  $[a^4\Pi_u]4s\sigma_g$  and  $[A^2\Pi_u]4s\sigma_g$  states are not observed in our total ion yield curve and  
197 if we use the average quantum defects of both of these series ( $\delta = 2.16 \pm 0.12$  and  $2.02 \pm 0.03$ ,  
198 respectively), we can estimate the appearance energies of both components. This would lead  
199 the  $[a^4\Pi_u]4s\sigma_g$  state to appear between 7.00 – 8.05 eV (56500 - 64900  $\text{cm}^{-1}$ ) and the  $[A^2\Pi_u]4s\sigma_g$   
200 state between 8.44 – 8.65 eV (68100 - 69800  $\text{cm}^{-1}$ ), well below the  $S_2$  ionization energy located  
201 at  $\sim 9.37$  eV. These energies are significantly higher than the B and B'' states of  $S_2$  [43] and the  
202 closest assignment (to our knowledge) of assigned Rydberg states in this region for  $S_2$  pertain  
203 to the  $C^3\Sigma^-$  Rydberg state but it was theorized by Cooper & Western that a quintet ion-pair state  
204 with an  $a^4\Pi_u$  ion core should lie around 72620  $\text{cm}^{-1}$  [43]. For the moment, the whereabouts of  
205 the  $n = 4$  components of the  $[a^4\Pi_u]ns\sigma_g$  and  $[A^2\Pi_u]ns\sigma_g$  Rydberg series remain up for  
206 discussion.

207 There are some Rydberg series that have been intentionally left out of the assignment  
 208 which are those of the three Rydberg series corresponding to an excitation to a d Rydberg  
 209 orbital, namely  $[a^4\Pi_u]nd\sigma_g$ ,  $[a^4\Pi_u]nd\delta_g$ ,  $[a^4\Pi_u]nd\pi_g$ ,  $[A^2\Pi_u]nd\sigma_g$ ,  $[A^2\Pi_u]nd\delta_g$ ,  $[A^2\Pi_u]nd\pi_g$ .

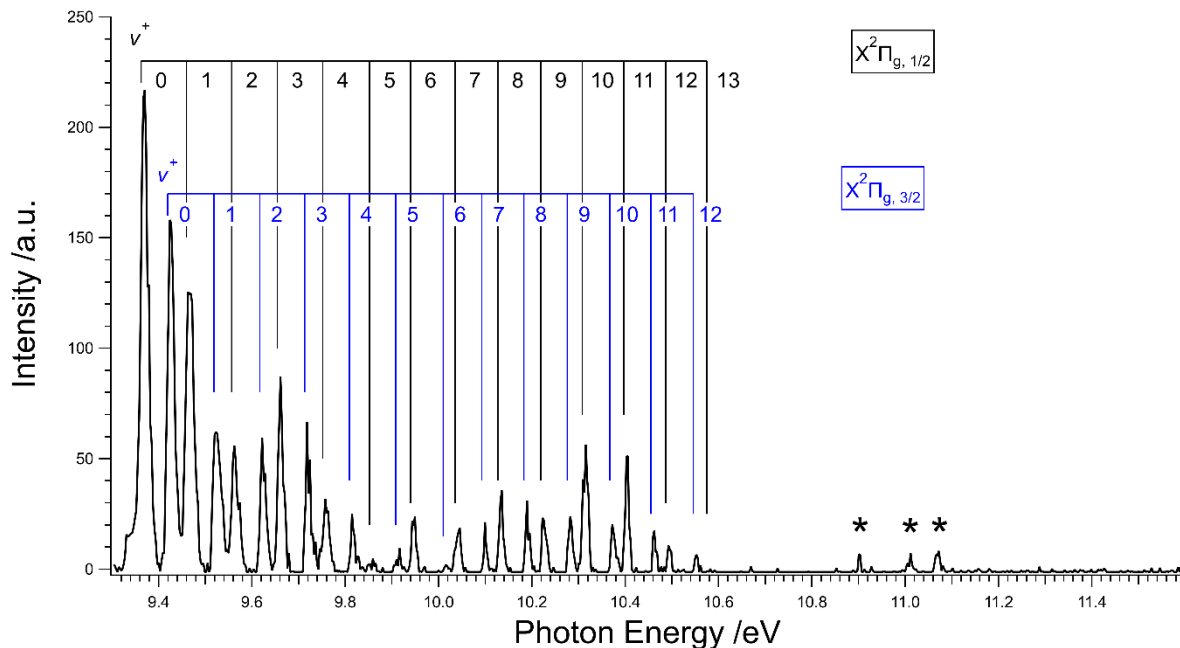
210 The quantum defect of d Rydberg-type orbitals are expected to be generally quite small  
 211 as the quantum defect of such orbitals for atomic sulfur was around 0.3. These states would thus  
 212 have expected onsets between 9.73 and 10.08 eV in the case of  $[a^4\Pi_u]3d\sigma_g$ ,  $[a^4\Pi_u]3d\delta_g$ , and  
 213  $[a^4\Pi_u]3d\pi_g$ , and 10.15 and 10.51 eV in the case of  $[A^2\Pi_u]3d\sigma_g$ ,  $[A^2\Pi_u]3d\delta_g$ ,  $[A^2\Pi_u]3d\pi_g$ . The  
 214 9.73 – 10.08 eV region in the TIY does exhibit some structure, but it is too weak for a definitive  
 215 assignment of the onsets of the  $[a^4\Pi_u]3d\sigma_g$ ,  $[a^4\Pi_u]3d\delta_g$ , and  $[a^4\Pi_u]3d\pi_g$  states. The 10.15 –  
 216 10.51 eV region on the other hand coincides with the vibrational progression of the  $[a^4\Pi_u]5s\sigma_g$   
 217 state, which forbids any further assignment of the d Rydberg series.

218

### 219 3.2 Threshold Photoelectron Spectrum (TPES)

#### 220 3.2.1 $X^2\Pi_{\Omega,g}$ ground state

221 The TPES of  $^{32}\text{S}_2$  is presented in Figure 3 from its first ionization threshold up to 11.5 eV. The  
 222 transitions assigned in Figure 3 are labeled by the final vibrational states of the cation (starting  
 223 from the neutral  $\text{S}_2$  ground state). The TPES of  $^{33}\text{S}^{32}\text{S}$  and  $^{34}\text{S}^{32}\text{S}$  are provided in Figure S1 of  
 224 the SI. The vibrational assignments of all isotopologues are given in Table 3.



225

226 **Figure 3.** TPES of  $^{32}\text{S}_2$ . Vibrational assignments of the  $X^2\Pi_{\Omega,g}$  ( $\Omega = 1/2, 3/2$ ) ground state are  
 227 presented in black and blue. A few outstanding peaks at 10.894 eV, 11.005 eV and 11.065 eV  
 228 labeled by asterisks remain unassigned for now.

229 **Table 3.** Vibrational and spin-orbit assignments of the final  $X^2\Pi_{\Omega, g} v$  ionic states. The values  
 230 have been corrected by the 5.4 meV Stark shift caused by the electric field (53 V·cm<sup>-1</sup>). The  
 231 errors of the peak positions are obtained by convoluting the photon energy accuracy (2 meV)  
 232 and the pointing accuracy which are on average smaller for <sup>32</sup>S<sub>2</sub> than the <sup>33</sup>S<sup>32</sup>S and <sup>34</sup>S<sup>32</sup>S  
 233 isotopologues due to the larger electron bandwidth used to create their TPES and their weaker  
 234 signal-to-noise ratio.

$\Pi_{\Omega, v}$		Energy <sup>32</sup> S <sub>2</sub>		Energy <sup>33</sup> S <sup>32</sup> S		Energy <sup>34</sup> S <sup>32</sup> S	
$\Omega$	$v$	eV	cm <sup>-1</sup>	eV	cm <sup>-1</sup>	eV	cm <sup>-1</sup>
1/2	0	9.371 ± 0.002	75580 ± 16	9.368 ± 0.002	75560 ± 17	9.369 ± 0.002	75564 ± 16
3/2	0	9.428 ± 0.002	76040 ± 16	9.428 ± 0.002	76040 ± 17	9.421 ± 0.002	75983 ± 16
1/2	1	9.469 ± 0.002	76369 ± 16	9.467 ± 0.002	76356 ± 17	9.466 ± 0.002	76349 ± 17
3/2	1	9.526 ± 0.002	76836 ± 17	9.525 ± 0.002	76823 ± 19	9.524 ± 0.002	76819 ± 18
1/2	2	9.565 ± 0.002	77149 ± 18	9.568 ± 0.002	77167 ± 18	9.564 ± 0.003	77139 ± 21
3/2	2	9.625 ± 0.002	77630 ± 17	9.622 ± 0.002	77603 ± 19	9.620 ± 0.003	77588 ± 20
1/2	3	9.663 ± 0.002	77937 ± 17	9.661 ± 0.002	77924 ± 18	9.658 ± 0.002	77895 ± 18
3/2	3	9.721 ± 0.002	78408 ± 17	9.721 ± 0.002	78408 ± 16	9.715 ± 0.003	78355 ± 21
1/2	4	9.761 ± 0.003	78725 ± 20	9.758 ± 0.003	78700 ± 28	9.756 ± 0.005	78689 ± 43
3/2	4	9.817 ± 0.002	79182 ± 17	9.818 ± 0.002	79190 ± 17	9.815 ± 0.002	79160 ± 20
1/2	5	9.852 ± 0.002	79462 ± 19	9.852 ± 0.002	79458 ± 19	9.858 ± 0.007	79513 ± 56
3/2	5	9.918 ± 0.002	79992 ± 17	9.915 ± 0.003	79972 ± 23	9.903 ± 0.002	79875 ± 19

1/2	6	9.949 ± 0.002	80240 ± 17	9.944 ± 0.002	80201 ± 16	9.938 ± 0.002	80159 ± 17
3/2	6	10.010 ± 0.003	80739 ± 21	10.007 ± 0.003	80715 ± 26	10.003 ± 0.002	80677 ± 18
1/2	7	10.044 ± 0.002	81014 ± 17	10.031 ± 0.002	80909 ± 18	10.034 ± 0.002	80933 ± 18
3/2	7	10.101 ± 0.002	81473 ± 16	10.100 ± 0.003	81465 ± 26	10.090 ± 0.002	81385 ± 16
1/2	8	10.135 ± 0.002	81747 ± 16	10.130 ± 0.002	81707 ± 17	10.125 ± 0.002	81667 ± 17
3/2	8	10.191 ± 0.002	82199 ± 16	10.187 ± 0.004	82167 ± 33	10.181 ± 0.002	82118 ± 19
1/2	9	10.227 ± 0.002	82490 ± 17	10.225 ± 0.002	82473 ± 16	10.214 ± 0.002	82385 ± 18
3/2	9	10.284 ± 0.002	82949 ± 16	10.280 ± 0.002	82917 ± 18	10.272 ± 0.002	82852 ± 16
1/2	10	10.316 ± 0.002	83207 ± 16	10.315 ± 0.002	83199 ± 17	10.301 ± 0.002	83086 ± 16
3/2	10	10.375 ± 0.002	83683 ± 16	10.369 ± 0.002	83635 ± 20	10.359 ± 0.002	83554 ± 16
1/2	11	10.405 ± 0.002	83925 ± 16	10.399 ± 0.002	83877 ± 18	10.389 ± 0.002	83796 ± 16
3/2	11	10.463 ± 0.002	84393 ± 17	10.460 ± 0.005	84369 ± 43	10.451 ± 0.002	84296 ± 17
1/2	12	10.495 ± 0.002	84651 ± 17	10.498 ± 0.002	84675 ± 17	10.475 ± 0.003	84490 ± 20
3/2	12	10.554 ± 0.002	85127 ± 17	10.548 ± 0.005	85079 ± 48	10.535 ± 0.002	84974 ± 17

235

236 On average, the observed spin-orbit (SO) splitting in the ground state is  $463 \pm 17 \text{ cm}^{-1}$ .

237 This value compares well with that observed by Dyke *et al.* ( $470 \pm 25 \text{ cm}^{-1}$ ) [17].

238 By assigning the vibrational energy levels of the  $X^2\Pi_{\Omega, g}$  ground state in the TPES, we  
 239 can derive the ground state spectroscopic constants, namely  $T_e$ ,  $\omega_e$ , and  $\omega_e x_e$ . To do this, we fit  
 240 the observed energy levels to obtain the values of  $T_e$ ,  $\omega_e$ , and  $\omega_e x_e$  that we present in Table 4.  
 241 We could not include the  $\omega_e y_e$  parameter in the fit without degrading the uncertainty of the other  
 242 parameters.

243

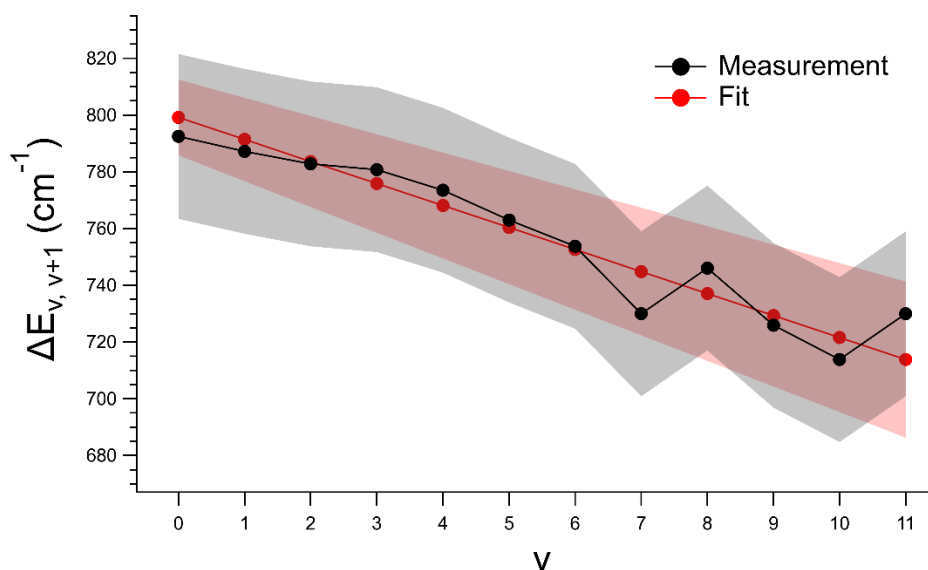
244 **Table 4.** Spectroscopic parameters pertaining to the two SO components of the  $X^2\Pi_{\Omega, g}$  ground  
 245 state of  $S_2^+$  and its isotopologues as obtained by including all of the observed vibrational levels.

$X^2\Pi_g$	$T_e$ [ $\text{cm}^{-1}$ ]	$\omega_e$ [ $\text{cm}^{-1}$ ]	$\omega_e x_e$ [ $\text{cm}^{-1}$ ]	Ref.
$^{32}\text{S}_2$	$75400 \pm 30$	$807 \pm 5$	$3.88 \pm 0.03$	This work
		806.099	3.3971	[23]
		805.9	3.38	[21]
$^{33}\text{S}^{32}\text{S}$	$75410 \pm 35$	$797 \pm 7$	$3.5 \pm 0.3$	This work
$^{34}\text{S}^{32}\text{S}$	$75380 \pm 35$	$805 \pm 7$	$4.7 \pm 0.4$	This work

246

247 In Figure 4 we compare the measured energy level spacing between adjacent spin-orbit  
 248 ladders of the  $X^2\Pi_{\Omega, g}$  ground state and the same energy level spacing using the fitted parameters  
 249 in Table 3. The agreement is good between  $\nu = 0 - 7$ , but the highest energy levels appear to  
 250 suffer from perturbation effects from an unknown ionic state. However, since the uncertainties  
 251 still overlap where the deviation in the energy level spacing is at its greatest, we cannot conclude  
 252 such a perturbation is present. Furthermore, the additional ionic states predicted by Yu *et al.*[27]  
 253 would have their onsets at least  $32000 \text{ cm}^{-1}$  above the onset of the ground state, i.e., around  
 254  $108000 \text{ cm}^{-1}$ , which is still approximately  $20000 \text{ cm}^{-1}$  higher than the alleged perturbation  
 255 effects. We can thus not conclude that the ground state is suffering from perturbation effects  
 256 from a hidden state.

257



258  
 259 **Figure 4.** Vibrational energy level spacings for the  $X^2\Pi_{\Omega, g}$  ground state are plotted in black.  
 260 The red line represents the energy level spacing calculated from the fitted parameters presented  
 261 in Table 3. Shaded regions denote the propagated uncertainties from the TPES for the  
 262 measurement (black), and the propagated uncertainties from the fitted parameters (red).

263  
 264 As the TPES of these isotopologues were much weaker than that of  $^{32}\text{S}_2$ , their fitted  
 265 parameters suffer from larger uncertainties which make any discussion of supposed  
 266 perturbations mute.

267 The unassigned peaks at 10.894 eV, 11.005 eV and 11.065 eV from Figure 3 can now  
 268 be tentatively assigned by using the derived spectroscopic parameters from the TPES as  
 269 presented in Table 4. By extrapolating the fitted values to higher  $v$  levels, we can tentatively  
 270 estimate that these peaks belong to the  $X^2\Pi_{3/2}(v = 16)$ ,  $X^2\Pi_{1/2}(v = 18)$  and  $X^2\Pi_{3/2}(v = 18)$   
 271 levels, respectively. This comes with the assumption that these levels are reasonably  
 272 unperturbed.

273 Regarding the peak intensities in the  $X^2\Pi_{\Omega, g}$  ground state, they do not follow a definite  
 274 Franck-Condon intensity trend. Between 10.0 and 10.6 eV, rather than decreasing  
 275 monotonously, the signals increase in intensity before decreasing and disappearing above 10.6  
 276 eV. This is due to the presence of autoionizing states that can enhance weak direct transitions  
 277 by indirect processes, because the vibrational overlap between the intermediate autoionizing  
 278 state and the final cation state may be more favorable for different cation equilibrium distances,  
 279 as seen in other systems [46]. Indeed, the first autoionization features—converging towards the  
 280  $a^4\Pi_u$  ionic state—are seen in Figure 2 to begin at 10.1 eV, which coincides with the departure  
 281 from the Franck-Condon behavior observed in the TPES of Figure 3. This explanation likewise



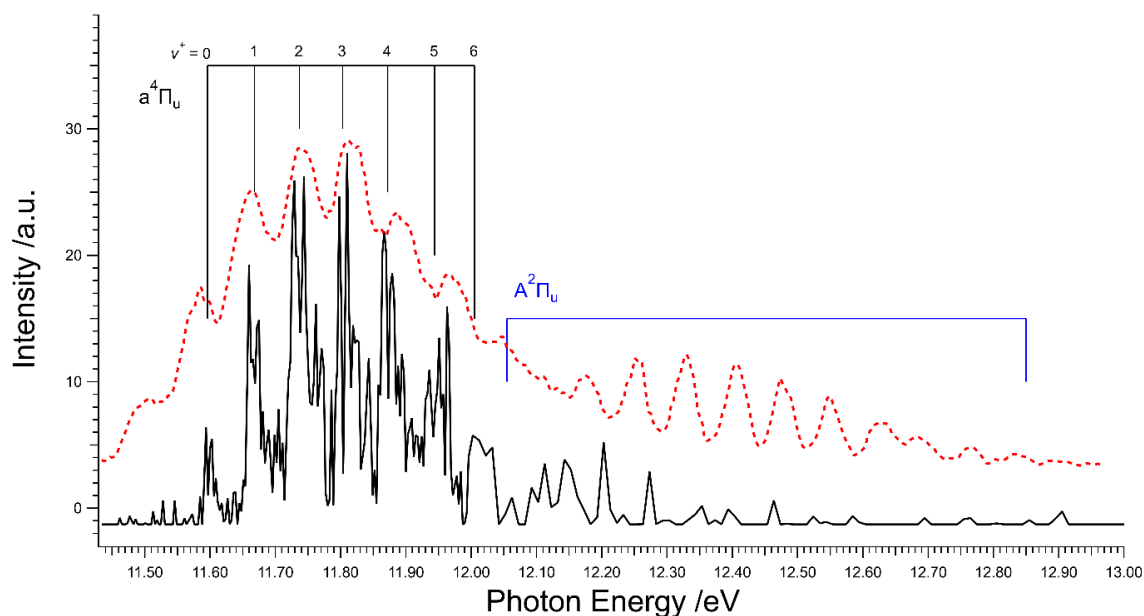
282 applies to the appearance of peaks belonging to the  $X^2\Pi_{3/2}(v = 16)$ ,  $X^2\Pi_{1/2}(v = 18)$  and  $X^2\Pi_{3/2}$   
283  $(v = 18)$  levels between 10.9 and 11.1 eV in the TPES, which coincides with the first  
284 autoionizing feature converging to the  $b^4\Sigma_g^-$  ionic state.

285

### 286 3.2.1 $S_2^+$ excited states

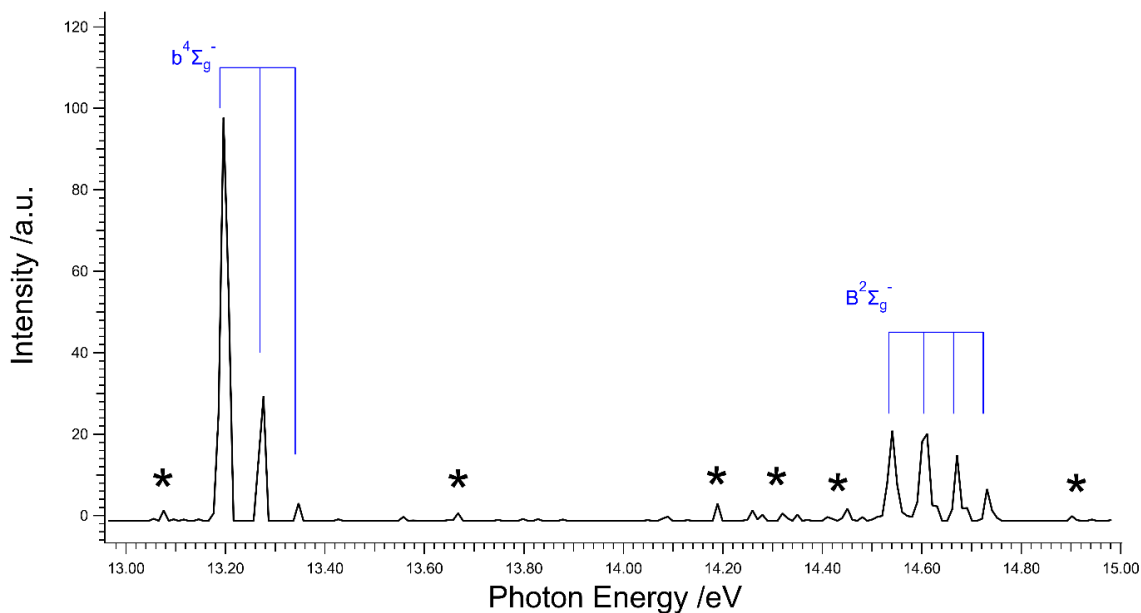
287 The TPES of  $S_2$  from 11.5 to 15.0 eV is presented in Figures 5 and 6 along with assignments  
288 corresponding to the final cationic states of  $S_2^+$ . The assigned spectroscopic parameters are  
289 presented in Table 5. Above 12.0 eV, we expected to see the spectral fingerprints of the  $A^2\Pi_u$   
290 state (akin to Dyke *et al.*) but the threshold electron signal used to make up the TPES was not  
291 strong enough to resolve it and thus our TPES forbids vibrational assignment of the  $A^2\Pi_u$  state.

292



293

294 **Figure 5.** TPES of  $S_2$  from 11.4 eV up to 12.9 eV. Up to 12.0 eV the step size of the TPES is 3  
295 meV, changing to 10 meV above 12.0. Band assignments of the  $a^4\Pi_u$ ,  $A^2\Pi_u$  states are depicted  
296 as well as comparison with the PES from Dyke *et al.*[17]



297  
 298 **Figure 6.** TPES of  $S_2$  from 13.0 eV up to 14.9 eV. Band assignments of the  $b^4\Sigma_g^-$ , and  $B^2\Sigma_g^-$   
 299 states are depicted. Unassigned peaks are denoted with asterisks.

300  
 301 **Table 5.** Spectroscopic parameters pertaining to the observed excited states of the  $S_2^+$  cation in  
 302 the TPES. Here,  $T_e$  and  $\omega_e$  (and  $\omega_e x_e$  in the case of  $B^2\Sigma_g^-$ ) were fitted to the observed line  
 303 positions in accordance with  $E = T_e + \omega_e(v + 1/2) - w_e x_e(v + 1/2)^2$ .  $E_0$  is the excitation energy of  
 304 the ionic states from the  $X^2\Pi_{\Omega, g}$  ground state.

	$T_e$ [ $\text{cm}^{-1}$ ]	$E_0$ [ $\text{cm}^{-1}$ ]	$\omega_e$ [ $\text{cm}^{-1}$ ]	$\omega_e x_e$ [ $\text{cm}^{-1}$ ]	Ref.
$a^4\Pi_u$	$93520 \pm 30$	$18470 \pm 30$ 19438	$550 \pm 10$ 620	-	This work [17]
$A^2\Pi_u$	$96950 \pm 50$	$21550 \pm 50$ 23551	- 547	- 3.1	This work [17]
$b^4\Sigma_g^-$	$106580 \pm 30$	$31770 \pm 30$ 30568	$608 \pm 20$ 581		This work [17]
$B^2\Sigma_g^-$	$117420 \pm 30$	$42440 \pm 30$ 42021	$508 \pm 20$ 546	$20 \pm 6$	This work [17]

305  
 306 Further comparison with the recorded PES from Dyke *et al.* does show the significantly  
 307 improved resolution on the  $a^4\Pi_u$  state as the quartet splitting of the  $a^4\Pi_u$ , state ( $\Omega = 1/2, 3/2,$   
 308  $5/2$ ) is clearly visible. Dyke *et al.* predicted a spin-orbit splitting of approximately  $160 \text{ cm}^{-1}$  or

309 20 meV. Here, we observe an average splitting of  $98 \pm 26 \text{ cm}^{-1}$  ( $12.1 \pm 3.2 \text{ meV}$ ) which is well  
310 below the resolution of the apparatus used by Dyke *et al.*

311 In Figure 6, we see clear signatures of the  $b^4\Sigma_g^-$ , and  $B^2\Sigma_g^-$  states. Between the  $b^4\Sigma_g^-$ ,  
312 and  $B^2\Sigma_g^-$  states there are several weak peaks that remain unassigned. In the case  $O_2^+$ , there are  
313 two ionic states found between the  $^4\Sigma_g^-$  and the  $^2\Sigma_g^-$ , namely  $^2\Phi_u$  and  $^2\Delta_g$  [47]. Indeed, some  
314 states are expected to have small oscillator strength coefficients ( $f > 0.01$ ), but may be weakly  
315 allowed by couplings with other states and thus show up as very faint signals in our recorded  
316 TPES. Another possibility is that these belong to one of the excited states calculated by Yu *et*  
317 *al.* [27] but without a clear spectral pattern, these peaks remain unassigned for now.

318

## 319 SUMMARY AND CONCLUSIONS

320 In light of recent progress on explaining the abundances (or lack thereof) of observed sulfur in  
321 the universe, we have investigated the photoionization spectroscopy and dynamics of the sulfur  
322 dimer,  $S_2$ . These include the first threshold photoelectron spectrum of  $S_2$  whose resolution is  
323 significantly improved as compared with previous photoelectron spectra [17]. We also collected  
324 the total ion yield of  $S_2^+$  with significantly higher resolution than previous measurements [26].  
325 The high-resolution TPES allows us to fit spectroscopic constants to the ionic states of  $S_2^+$  with  
326 higher accuracy and, in turn, guides the assignment of the very rich total ion yield curve  
327 exhibiting numerous autoionization features. Interestingly, these autoionization processes also  
328 lead to a more precise mapping of the potential energy surface of the  $X^2\Pi_{\Omega, g}$  ground cation  
329 state because highly excited vibrational states on the cation can now be accessed indirectly via  
330 Rydberg states.

331 Some unexplored features in the TPES are still observed around the  $b^4\Sigma_g^-$  and the  $B^2\Sigma_g^-$   
332 excited states of the cation. These could be due to *e.g.*, other excited states that have been  
333 predicted at higher energies [27], hot bands or even ionization of metastable states of neutral  
334  $S_2$ .

335

## 336 ACKNOWLEDGMENTS

337 We warmly thank the whole SOLEIL staff for running smoothly the facility under project  
338 99180002. We are indebted to JF Gil for his help on the SAPHIRS chamber. We also thank  
339 Prof. J. Liévin for very constructive discussions. The research described in this work has  
340 received financial support from the French Agence Nationale de la Recherche (ANR) under

341 Grant No. ANR-12-BS08-0020-02 (project SYNCHROKIN). H. R. H. is grateful for support  
342 from the Marie Skłodowska Curie Actions, proposal ID: 838372.

343

344 **REFERENCES**

- 345 [1] S. Black, *The Biochemistry of Sulfur-Containing Compounds*, *Annu. Rev. Biochem.* 32  
346 (1963) 399–418. <https://doi.org/10.1146/annurev.bi.32.070163.002151>.
- 347 [2] E.B. Jenkins, *A Unified Representation of Gas-Phase Element Depletions in the*  
348 *Interstellar Medium*, *ApJ.* 700 (2009) 1299–1348. [https://doi.org/10.1088/0004-](https://doi.org/10.1088/0004-637X/700/2/1299)  
349 [637X/700/2/1299](https://doi.org/10.1088/0004-637X/700/2/1299).
- 350 [3] M.F. Ahearn, D.G. Schleicher, P.D. Feldman, *The discovery of S<sub>2</sub> in comet IRAS-Araki-*  
351 *Alcock 1983d*, *ApJ.* 274 (1983) L99. <https://doi.org/10.1086/184158>.
- 352 [4] S.J. Kim, M.F. A’Hearn, D.D. Wellnitz, R. Meier, Y.S. Lee, *The rotational structure of*  
353 *the B–X system of sulfur dimers in the spectra of Comet Hyakutake (C/1996 B2)*, *Icarus.*  
354 166 (2003) 157–166. <https://doi.org/10.1016/j.icarus.2003.07.003>.
- 355 [5] K.S. Noll, M.A. McGrath, L.M. Trafton, S.K. Atreya, J.J. Caldwell, H.A. Weaver, R.V.  
356 Yelle, C. Barnet, S. Edgington, *HST spectroscopic observations of Jupiter after the*  
357 *collision of comet Shoemaker-Levy 9*, *Science.* 267 (1995) 1307–1313.  
358 <https://doi.org/10.1126/science.7871428>.
- 359 [6] J.R. Spencer, K.L. Jessup, M.A. McGrath, G.E. Ballester, R. Yelle, *Discovery of Gaseous*  
360 *S<sub>2</sub> in Io’s Pele Plume*, *Science.* 288 (2000) 1208–1210.  
361 <https://doi.org/10.1126/science.288.5469.1208>.
- 362 [7] K.L. Jessup, J. Spencer, R. Yelle, *Sulfur volcanism on Io*, *Icarus.* 192 (2007) 24–40.  
363 <https://doi.org/10.1016/j.icarus.2007.06.025>.
- 364 [8] K. Zahnle, M.S. Marley, R.S. Freedman, K. Lodders, J.J. Fortney, *Atmospheric Sulfur*  
365 *Photochemistry on Hot Jupiters*, *ApJ.* 701 (2009) L20–L24. [https://doi.org/10.1088/0004-](https://doi.org/10.1088/0004-637X/701/1/L20)  
366 [637X/701/1/L20](https://doi.org/10.1088/0004-637X/701/1/L20).
- 367 [9] J.C. Laas, P. Caselli, *Modeling sulfur depletion in interstellar clouds*, *A&A.* 624 (2019)  
368 A108. <https://doi.org/10.1051/0004-6361/201834446>.
- 369 [10] T.H.G. Vidal, J.-C. Loison, A.Y. Jaziri, M. Ruaud, P. Gratier, V. Wakelam, *On the*  
370 *reservoir of sulphur in dark clouds: chemistry and elemental abundance reconciled*,  
371 *Monthly Notices of the Royal Astronomical Society.* 469 (2017) 435–447.  
372 <https://doi.org/10.1093/mnras/stx828>.
- 373 [11] L.F. Rodríguez-Almeida, I. Jiménez-Serra, V.M. Rivilla, J. Martín-Pintado, S. Zeng,  
374 B. Tercero, P. de Vicente, L. Colzi, F. Rico-Villas, S. Martín, M.A. Requena-Torres,  
375 *Thiols in the Interstellar Medium: First Detection of HC(O)SH and Confirmation of*  
376 *C<sub>2</sub>H<sub>5</sub>SH*, *ApJL.* 912 (2021) L11. <https://doi.org/10.3847/2041-8213/abf7cb>.
- 377 [12] J. Cernicharo, C. Cabezas, M. Agúndez, B. Tercero, J.R. Pardo, N. Marcelino, J.D.  
378 Gallego, F. Tercero, J.A. López-Pérez, P. de Vicente, *TMC-1, the starless core sulfur*  
379 *factory: Discovery of NCS, HCCS, H<sub>2</sub>CCS, H<sub>2</sub>CCCS, and C<sub>4</sub>S and detection of C<sub>5</sub>S*,  
380 *A&A.* 648 (2021) L3. <https://doi.org/10.1051/0004-6361/202140642>.
- 381 [13] J. Cernicharo, C. Cabezas, Y. Endo, N. Marcelino, M. Agúndez, B. Tercero, J.D.  
382 Gallego, P. de Vicente, *Space and laboratory discovery of HC<sub>3</sub>S<sup>+</sup>*, *A&A.* 646 (2021) L3.  
383 <https://doi.org/10.1051/0004-6361/202040013>.
- 384 [14] M. Agúndez, N. Marcelino, J. Cernicharo, M. Tafalla, *Detection of interstellar HCS*  
385 *and its metastable isomer HSC: new pieces in the puzzle of sulfur chemistry*, *A&A.* 611  
386 (2018) L1. <https://doi.org/10.1051/0004-6361/201832743>.
- 387 [15] J. Cernicharo, B. Lefloch, M. Agúndez, S. Bailleux, L. Margulès, E. Roueff, R.  
388 Bachiller, N. Marcelino, B. Tercero, C. Vastel, E. Caux, *Discovery of the Ubiquitous*  
389 *Cation NS<sup>+</sup> in Space Confirmed by Laboratory Spectroscopy*, *The Astrophysical Journal*  
390 *Letters.* 853 (2018) L22. <https://doi.org/10.3847/2041-8213/aaa83a>.
- 391 [16] C.N. Shingledecker, T. Lamberts, J.C. Laas, A. Vasyunin, E. Herbst, J. Kaestner, P.  
392 Caselli, *Efficient Production of S<sub>8</sub> in Interstellar Ices: The effects of cosmic ray-driven*

- 393 radiation chemistry and non-diffusive bulk reactions, *ApJ*. 888 (2020) 52.  
 394 <https://doi.org/10.3847/1538-4357/ab5360>.
- 395 [17] J.M. Dyke, L. Golob, N. Jonathan, A. Morris, Vacuum ultraviolet photoelectron  
 396 spectroscopy of transient species. Part 5.—The  $S_2(^3\Sigma_g^-)$  molecule | Semantic Scholar,  
 397 *Journal of the Chemical Society, Faraday Transactions*. 71 (1975) 1026–1036.  
 398 <https://doi.org/10.1039/F29757101026>.
- 399 [18] J. Berkowitz, PES of high temperature vapors. VII.  $S_2$  and  $Te_2$ , *Journal of Chemical*  
 400 *Physics*. 62 (1975) 4074–4079. <https://doi.org/10.1063/1.430283>.
- 401 [19] M. Tsuji, I. Murakami, Y. Nishimura, A new emission produced from sulfur  
 402 monochloride in a helium afterglow:  $S_2^+(A^2\Pi_u-X^2\Pi_g)$ , *Chemical Physics Letters*. 75  
 403 (1980) 536–539. [https://doi.org/10.1016/0009-2614\(80\)80572-0](https://doi.org/10.1016/0009-2614(80)80572-0).
- 404 [20] M. Tsuji, I. Murakami, Y. Nishimura, UV and visible emission produced from  $S_2Cl_2$   
 405 in the rare gas flowing afterglow, *J. Chem. Phys.* 75 (1981) 5373–5380.  
 406 <https://doi.org/10.1063/1.441982>.
- 407 [21] A.J. Capel, J.H.D. Eland, R.F. Barrow, Rotational analysis of the A—X bands of  $S_2^+$ ,  
 408 *Chemical Physics Letters*. 82 (1981) 496–500. [https://doi.org/10.1016/0009-](https://doi.org/10.1016/0009-2614(81)85427-9)  
 409 [2614\(81\)85427-9](https://doi.org/10.1016/0009-2614(81)85427-9).
- 410 [22] W. Rosinger, M. Grade, W. Hirschwald, Electron Impact Induced Excitation Processes  
 411 Involving the Sulfur Clusters  $S_2$  to  $S_8$ , *Berichte Der Bunsengesellschaft Für Physikalische*  
 412 *Chemie*. 87 (1983) 536–542. <https://doi.org/10.1002/bbpc.19830870616>.
- 413 [23] K. Brabaharan, J.A. Coxon, Rotational analysis of the  $A^2\Pi_u \rightarrow X^2\Pi_g$  system of  $^{32}S_2^+$ ,  
 414 *Journal of Molecular Spectroscopy*. 128 (1988) 540–553. [https://doi.org/10.1016/0022-](https://doi.org/10.1016/0022-2852(88)90169-5)  
 415 [2852\(88\)90169-5](https://doi.org/10.1016/0022-2852(88)90169-5).
- 416 [24] C.-C. Zen, Y.-P. Lee, J.F. Ogilvie, Spectra of the vibronic transition A-X of  $S_2^+$  in  
 417 solid neon, *Spectrochimica Acta Part A: Molecular and Biomolecular Spectroscopy*. 52  
 418 (1996) 1727–1735. [https://doi.org/10.1016/S0584-8539\(96\)01734-5](https://doi.org/10.1016/S0584-8539(96)01734-5).
- 419 [25] V.I. Gerasimova, Yu.S. Zavorotny, A.O. Rybaltovskii, P.V. Chernov, O.D. Sazhin,  
 420 R.R. Khrapko, A.A. Frolov, Color Centers in Sulfur-Doped Silica Glasses: Spectroscopic  
 421 Manifestations of an  $S_2^+$  Interstitial Molecular Ion, *Glass Physics and Chemistry*. 28  
 422 (2002) 5–10. <https://doi.org/10.1023/A:1014241211374>.
- 423 [26] C.L. Liao, C.Y. Ng, Molecular beam photoionization study of  $S_2$ , *J. Chem. Phys.* 84  
 424 (1986) 778–782. <https://doi.org/10.1063/1.450576>.
- 425 [27] W. Yu, Z. Zhu, C. Chuncai, S. Deheng, A theoretical investigation of the  $S_2^+$  cation in  
 426 the gas phase, *Canadian Journal of Chemistry*. (2014). [https://doi.org/10.1139/cjc-2014-](https://doi.org/10.1139/cjc-2014-0255)  
 427 [0255](https://doi.org/10.1139/cjc-2014-0255).
- 428 [28] L.R. Varas, L.H. Coutinho, R.B. Bernini, A.M. Betancourt, C.E.V. de Moura, A.B.  
 429 Rocha, G.G.B. de Souza, Breaking the disulfide chemical bond using high energy  
 430 photons: the dimethyl disulfide and methyl propyl disulfide molecules, *RSC Adv.* 7  
 431 (2017) 36525–36532. <https://doi.org/10.1039/C7RA05001A>.
- 432 [29] T. Baer, R.P. Tuckett, Advances in threshold photoelectron spectroscopy (TPES) and  
 433 threshold photoelectron photoion coincidence (TPEPICO), *Phys. Chem. Chem. Phys.* 19  
 434 (2017) 9698–9723. <https://doi.org/10.1039/C7CP00144D>.
- 435 [30] L. Nahon, N. de Oliveira, G.A. Garcia, J.-F. Gil, B. Pilette, O. Marcouille, B. Lagarde,  
 436 F. Polack, DESIRS: a state-of-the-art VUV beamline featuring high resolution and  
 437 variable polarization for spectroscopy and dichroism at SOLEIL, *Journal of Synchrotron*  
 438 *Radiation*. 19 (2012) 508–520. <https://doi.org/10.1107/S0909049512010588>.
- 439 [31] X. Tang, G.A. Garcia, J.-F. Gil, L. Nahon, Vacuum upgrade and enhanced  
 440 performances of the double imaging electron/ion coincidence end-station at the vacuum  
 441 ultraviolet beamline DESIRS, *Review of Scientific Instruments*. 86 (2015).  
 442 <https://doi.org/10.1063/1.4937624>.

- 443 [32] G.A. Garcia, B.K.C. de Miranda, M. Tia, S. Daly, L. Nahon, DELICIOUS III: A  
 444 multipurpose double imaging particle coincidence spectrometer for gas phase vacuum  
 445 ultraviolet photodynamics studies, *Review of Scientific Instruments*. 84 (2013).  
 446 <https://doi.org/10.1063/1.4807751>.
- 447 [33] B. Mercier, M. Compin, C. Prevost, G. Bellec, R. Thissen, O. Dutuit, L. Nahon,  
 448 Experimental and theoretical study of a differentially pumped absorption gas cell used as  
 449 a low energy-pass filter in the vacuum ultraviolet photon energy range, *Journal of*  
 450 *Vacuum Science & Technology A-Vacuum Surfaces and Films*. 18 (2000) 2533–2541.  
 451 <https://doi.org/10.1116/1.1288196>.
- 452 [34] O. Marcouille, P. Brunelle, O. Chubar, F. Marteau, M. Massal, L. Nahon, K. Tavakoli,  
 453 J. Veteran, J.-M. Filhol, Design, construction and magnetic measurements of the HU640  
 454 (OPHELIE2) undulator dedicated to the DESIRS VUV beamline at SOLEIL, in: Choi, JY  
 455 and Rah, S (Ed.), *Synchrotron Radiation Instrumentation Pts 1 & 2*, American Institute of  
 456 Physics, 2 Huntington Quadrangle, Ste 1No1, Melville, NY 11747-4501 USA, 2007: p.  
 457 311+.
- 458 [35] G.A. Garcia, X. Tang, J.-F. Gil, L. Nahon, M. Ward, S. Batut, C. Fittschen, C.A.  
 459 Taatjes, D.L. Osborn, J.-C. Loison, Synchrotron-based double imaging  
 460 photoelectron/photoion coincidence spectroscopy of radicals produced in a flow tube: OH  
 461 and OD, *J. Chem. Phys.* 142 (2015) 164201. <https://doi.org/10.1063/1.4918634>.
- 462 [36] H.R. Hrodmarsson, G.A. Garcia, L. Nahon, J.-C. Loison, B. Gans, The absolute  
 463 photoionization cross section of the mercapto radical (SH) from threshold up to 15.0 eV,  
 464 *Phys. Chem. Chem. Phys.* 21 (2019) 25907–25915. <https://doi.org/10.1039/C9CP05809E>.
- 465 [37] G. Garcia, L. Nahon, I. Powis, Two-dimensional charged particle image inversion  
 466 using a polar basis function expansion, *Review of Scientific Instruments*. 75 (2004) 4989–  
 467 4996. <https://doi.org/10.1063/1.1807578>.
- 468 [38] H.R. Hrodmarsson, G.A. Garcia, L. Nahon, J.-C. Loison, B. Gans, Threshold  
 469 Photoelectron Spectrum of the Anilino Radical, *The Journal of Physical Chemistry A*. 123  
 470 (2019) 9193–9198. <https://doi.org/10.1021/acs.jpca.9b07273>.
- 471 [39] H.R. Hrodmarsson, J.-C. Loison, U. Jacovella, D.M.P. Holland, S. Boye-Peronne, B.  
 472 Gans, G.A. Garcia, L. Nahon, S.T. Pratt, Valence-Shell Photoionization of C<sub>4</sub>H<sub>5</sub>: The 2-  
 473 Butyn-1-yl Radical, *Journal of Physical Chemistry A*. 123 (2019) 1521–1528.  
 474 <https://doi.org/10.1021/acs.jpca.8b11809>.
- 475 [40] E. Lindholm, Rydberg Series in Small Molecules .i. Quantum Defects in Rydberg  
 476 Series, *Arkiv for Fysik*. 40 (1969) 97-.
- 477 [41] K. Yoshino, Y. Tanaka, Absorption spectrum of krypton in the vacuum uv region, *J.*  
 478 *Opt. Soc. Am.* 69 (1979) 159. <https://doi.org/10.1364/JOSA.69.000159>.
- 479 [42] K. Yoshino, Absorption Spectrum of the Argon Atom in the Vacuum-Ultraviolet  
 480 Region, *J. Opt. Soc. Am.* 60 (1970) 1220. <https://doi.org/10.1364/JOSA.60.001220>.
- 481 [43] M.J. Cooper, C.M. Western, Two-colour double resonance multiphoton ionisation  
 482 spectroscopy of S<sub>2</sub>, *Chemical Physics Letters*. 267 (1997) 365–369.  
 483 [https://doi.org/10.1016/S0009-2614\(97\)00099-7](https://doi.org/10.1016/S0009-2614(97)00099-7).
- 484 [44] O. Edqvist, E. Lindholm, L.E. Selin, L. Åsbrink, On the Photoelectron Spectrum of  
 485 O<sub>2</sub>, *Phys. Scr.* 1 (1970) 25–30. <https://doi.org/10.1088/0031-8949/1/1/004>.
- 486 [45] C.-S. Lam, H. Wang, Y. Xu, K.-C. Lau, C.Y. Ng, A vacuum-ultraviolet laser pulsed  
 487 field ionization-photoelectron study of sulfur monoxide (SO) and its cation (SO<sup>+</sup>), *The*  
 488 *Journal of Chemical Physics*. 134 (2011) 144304. <https://doi.org/10.1063/1.3575227>.
- 489 [46] M. Briant, L. Poisson, M. Hochlaf, P. de Pujo, M.-A. Gaveau, B. Soep, Ar<sub>2</sub>  
 490 Photoelectron Spectroscopy Mediated by Autoionizing States, *Phys. Rev. Lett.* 109 (2012)  
 491 193401. <https://doi.org/10.1103/PhysRevLett.109.193401>.

492 [47] F. Merkt, P.M. Guyon, J. Hepburn, High-resolution threshold photoelectron spectrum  
493 of molecular oxygen, *Chemical Physics*. 173 (1993) 479–484.  
494 [https://doi.org/10.1016/0301-0104\(93\)80162-3](https://doi.org/10.1016/0301-0104(93)80162-3).  
495